Effects of Mechanical Activation on the Formation and Sintering Kinetics of Barium Strontium Titanate Ceramics

Darko Kosanović[1*)], Nebojša J. Labus[1], Jelena Živojinović[1], Adriana Peleš Tadić[1], Vladimir A. Blagojević[1], Vladimir B. Pavlović[2]

[1]Institute of Technical Sciences of the Serbian Academy of Sciences and Arts, Knez Mihailova 35/IV, 11000 Belgrade, Serbia
[2]University of Belgrade, Faculty of Agriculture, Nemanjina 6, 11080 Belgrade, Serbia

Abstract:

The influence of mechanical activation on the formation, sintering kinetics and morphology was investigated in sintered barium strontium titanate (BST) ceramics with different Ba-to-Sr ratios. Initial powders were mechanically activated for 20 and 120 min, leading to mechano-chemical reaction and formation of $Ba_xSr_{1-x}TiO_3$ phases. Agglomeration was found to represent an important factor in the process of formation of $Ba_xSr_{1-x}TiO_3$ phases around 800 ⁰C and during sintering. It reduces the effectiveness of mechanical activation on formation of $Ba_xSr_{1-x}TiO_3$ phases beyond the short period (20 min), while in the process of sintering, prolonged mechanical activation (120 min) leads to a significant reduction in sintering temperature and the corresponding value of activation energy. In addition, all three systems show a phase transformation around 1100 ⁰C, attributed to the hexagonal-to-cubic phase transition. Morphology of the final sintered ceramics can be correlated primarily with the state of the pre-sintered powder, where mechanically activated powders with smaller particle size produced more compact and less porous final product.

Keywords: Ceramics; Sintering; Kinetics; Scanning electron microscopy; Phase transition.

1. Introduction

Since the discovery of the ferroelectric effect in barium strontium titanate $(Ba,Sr)TiO_3$, studies of BST materials have been a widely welcomed topic due to its high permittivity, low dielectric loss, high tunability coefficient, high reaction velocity, anti-breakdown ability, and simple fabrication process, etc. As an additional advantage, BST family is lead-free, and therefore compliant with current requirements for environmentally benign materials [1], making it very attractive for potential applications as piezoelectric transducers, dynamic random access memory (DRAM), tunable microwave devices, and an electrical energy storage unit [1-5]. Miniaturization of electronic devices requires synthesis of nanoscaled ferroelectric structures with significantly altered properties. These structures are interesting because of their piezoelectric properties, i.e. for miniaturization of piezoelectric sensors, which are used, for example, in medicine and ultrasonic devices and for the development of adjustable components for radio (RF) and microwave frequencies (e.g., adjustable filters, phase shifters, etc.) [6-8]. In addition, the dielectric permittivity of BST can be controlled by altering the electric field in which the dielectric is positioned. Barium strontium titanate (BST) is a solid solution family composed of barium titanate and strontium

_____

*)**Corresponding author:** darko.kosanovic@itn.sanu.ac.rs; kosanovic.darko@gmail.com

_____

titanate with its curie temperature covering a wide range. BST is a continuous solid solution with a tetragonal structure and the temperature of the phase transition from the ferroelectric phase to a paraelectric phase is determined by the substitution of Ba^{2+} by Sr^{2+} in the A-site of the perovskite structure (ABO_3) [9-12]. The variation of T_C in BST is determined by changes in the cell volume, where the change of the order and the diffuseness of the phase transition in BST could be attributed to a cell volume effect, with the mechanism of successive transitions of BST most likely similar to that of $BaTiO_3$ [13].

There are several methods for the synthesis of BST powder, either with a dry or wet chemical way of synthesis. The latter include co-precipitation, spray pyrolysis, and sol-gel techniques [14-21]. Each of these methods has its advantages and disadvantages. Typical advantages of the wet route are high purity, super fine powder production, good fluidity, low agglomeration, and lower sintering temperatures. Disadvantages include high-temperature calcinations (from 1000 to 1200 ^{o}C), the use of larger amounts of the initial powder, as well as large grain size, which cannot be used for the production of materials with high dielectric constant and high-porosity [22-24]. BST ceramics prepared by traditional solid-state reaction are usually sintered at 1350-1400 ^{o}C [25] and exhibit strong temperature sensitivity within a temperature range near the phase transition, which blocks its application and development. Also, this method results in homogeneous microstructure with large grain size [26], leading to high microwave loss. A sol-gel process has been proven to be very effective in controlling the size and shape of particles [27]. Recently, fine-grained BST (or nanocrystalline) ceramics were found to exhibit improved temperature stability and lower sintering temperature [28]. Compared with the coarse-grained ceramics prepared traditionally, nano-grained ceramics fabricated via chemical routes like sol-gel or/and citrate methods exhibited broad dielectric peaks, possessing better thermal stability, but its dielectric loss values were high [29-31]. However, the sol-gel process utilizes expensive precursors and requires careful control of the atmosphere. The co-precipitation process is limited to cation solutions with similar solubility products. Q. Chen et al. and U. Gesenhues reported that this method seems to be simple and effective since it has the advantage of being feasible, reproducible, environmental-benign and economic [32, 33]. In addition, there are also hydrothermal synthesis that are commercially used for the production of a given material by Miao, Zhou and Simões [34-38], where, it is often used due to its simplicity, allowing the control of grain size, morphology and degree of crystallinity by easy changes in the parameters of the experimental procedure.

Dry synthesis methods are based on the reactions in the solid state and are the most widely used methods for obtaining a BST [22-24]. These include reaction sintering, where the calcination step can be bypassed and a mixture of raw materials is sintered directly [39]. However, in order to facilitate the sintering, it is necessary to use mechanically activated precursor powders. In our research, we focused on the influence of mechanical activation on the formation and sintering of single phase BST, under different compositions of the precursor powder mixture. Sintering of powder mixtures has been widely used to obtain new materials and composites [40], while mechanical activation has been known to facilitate sintering of a variety of functional materials [41], providing better homogeneity of the starting powders, and is relatively simple and economical at the same time. It also has the advantages of lowering both the calcination temperature ($T_{cal} = 800$ °C) and sintering temperature.

2. Materials and Experimental Procedures

For the synthesis of barium strontium titanate ($BaSrTiO_3$, BST) system following commercially available $BaCO_3$ (99.8 % Aldrich), $SrCO_3$ (99.8 % Aldrich) and TiO_2 (99.99 % Aldrich) powders were mixed and homogenized in three different ratios of Ba and Sr (80/20, 50/50, 20/80 and mass% Ba to Sr). The mixtures were mechanically activated in a high-energy planetary ball mill (Fritsch Pulverisette 5). The process of milling was performed for 0

_____

to 120 minutes (0, 20, 40 and 120 min) in the air. Initial samples were milled in 500 cm³ zirconium oxide beakers together with balls of 10 mm in diameter (the ratio of powder and balls was 1:20). After milling, the powders were dried and calcined at a temperature of 800 °C, for 3 h inside a chamber furnace.

Compaction of powders was performed in a uniaxial double-sided mode, providing green bodies with the cylindrical shape with a diameter of 8 mm on hydraulic press RING, P-14 (VEB THURINGER). Pellets were compacted under 392 MPa pressure. They were treated nonisothermally in a dilatometer (Bähr Gerätebau GmbH Type 802s) at a heating rate of 10, 15, and 20 °C/min up to 1300 °C, followed by isothermal holding at 1300 °C for 30 min.

The microstructural characterization of the BST powders was performed by a Scanning Electron Microscope (SEM, JSM-6390 LV JEOL, 13, 15 and 20 kV). Before microstructure characterization, the samples were coated with gold in a sputter coater (SCD 005; BALTEC, Scotia, NY).

The X-ray powder diffraction patterns were obtained using Rigaku Ultima IV X-ray diffraction (XRD) instrument in thin film geometry with a grazing incidence angle of 0.5°, using Ni-filtered CuKα radiation ($\lambda = 1.54178$ Å). Diffraction data were acquired over the scattering angle 2θ from 10 to 70° with a step of 0.05° and acquisition rate of 2°/min and obtained data were analyzed with PDXL 2 software. Rietveld analysis was performed with full refinement using GSAS II software package [42]. Obtained values of R_{wp} (weighted residual factor) varied from 11.0 to 18.3 % and the Goodness of Fit indicator was GoF~1.

A thermogravimetric and differential thermal analysis (TG–DTA) of BST samples was determined by simultaneous TG–DTA (Setsys, SETARAM Instrumentation, Caluire, France) in the temperature range between 25 and 1300 °C under the air flow of 20 ml·min⁻¹, in an alumina pan. The heating profile was set as follows: the material was stabilized at 25 °C for 5 min then heated to 1300 °C with the heating rate of 10 °C min⁻¹.

3. Results and Discussion

Fig. 1 shows XRD patterns of BST precursor samples of different composition, mechanically activated for different periods of time. Rietveld analysis of these patterns (Table I) indicates that the process of mixing and homogenization of precursor BaO, TiO_2 and $SrCO_3$ powders produces a solid-state chemical reaction resulting in $Ba_xSr_{1-x}TiO_3$ phases for samples with 50 and 80 wt.% of strontium even before the application of heat.

Tab. I Rietveld analysis of mechanically activated samples after mixing and homogenization.

Sample	Dominant Phases	a (Å)	size	Strain	Wt.% $Ba_xSr_{1-x}TiO_3$
BST82-0	$Ba_{0.5}Sr_{0.5}CO_3/TiO_2$	/	79/55± 20	0.10/0.20 ± 0.05	/
BST82-20	$Ba_{0.5}Sr_{0.5}CO_3/TiO_2$	/	45/48± 14	0.3/0.3± 0.1	/
BST82-120	$Ba_{0.8}Sr_{0.2}TiO_3$	4.0058± 0.0005	42 ± 17	0.6 ± 0.1	84 ± 1
BST55-0	$Ba_{0.5}Sr_{0.5}TiO_3$	3.9482± 0.0007	60 ± 18	0.9 ± 0.2	63 ± 2
BST55-20	$Ba_{0.5}Sr_{0.5}TiO_3$	3.9565± 0.0004	64 ± 15	0.36 ± 0.04	87 ± 1
BST55-120	$Ba_{0.5}Sr_{0.5}TiO_3$	3.9525± 0.0004	71 ± 6	0.32 ± 0.06	92 ± 1
BST28-0	$Ba_{0.256}Sr_{0.744}TiO_3$	3.9066± 0.0008	86 ± 16	0.13 ± 0.03	38 ± 3
BST28-20	$Ba_{0.256}Sr_{0.744}TiO_3$	3.9196± 0.0004	34 ± 7	0.17 ± 0.06	85 ± 1
BST28-120	$Ba_{0.256}Sr_{0.744}TiO_3$	3.9178± 0.0004	35 ± 3	0.21 ± 0.03	90 ± 1

_____

In the sample with 80 wt.% of Ba, the dominant phases on mixing were $Ba_{0.5}Sr_{0.5}CO_3$ and TiO_2. Mechanical activation further increased the phase content of $Ba_xSr_{1-x}TiO_3$ phases and, at 120 minutes of activation, resulted in 84-92 wt.% of the corresponding $Ba_xSr_{1-x}TiO_3$ phase in all three samples with different Ba:Sr ratios. This indicates that the formation of $Ba_xSr_{1-x}TiO_3$ phases is possible through the mechano-chemical synthesis of BaO, TiO_2, and $SrCO_3$ nanopowders, with powder mixture with 1:1 ratio of Ba:Sr providing higher yields than the samples with 80 % Sr and Ba, respectively.
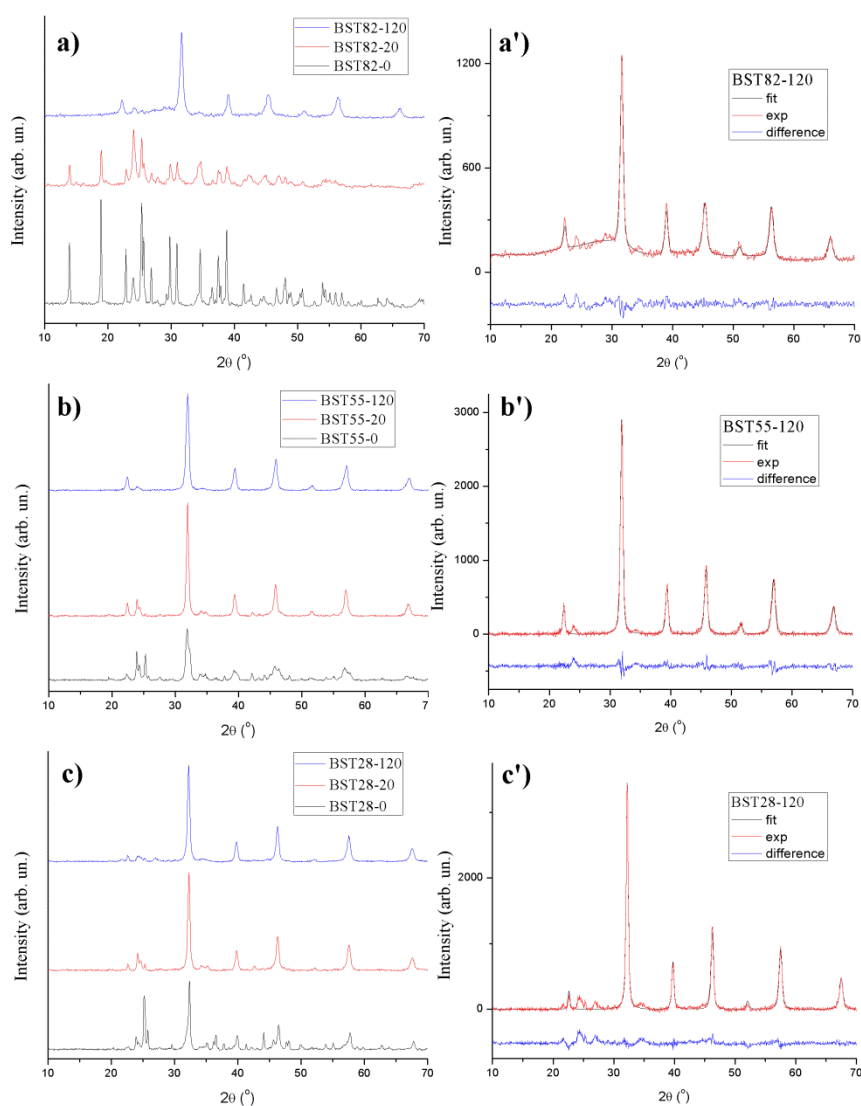
Fig. 1. XRD spectra of samples a) BST82 b) BST55 and c) BST28 for activation times of 0, 20, and 120 minutes, with Rietveld analysis shown for samples activated for 120 min (a', b', c').

$Ba_{0.8}Sr_{0.2}TiO_3$ phase is a tetragonal phase (P4mm) where the Ti atom is located slightly off-center in a cubic Ba/Sr-O structure, similar to $BaTiO_3$ [41]. Both $Ba_{0.5}Sr_{0.5}TiO_3$ and $Ba_{0.256}Sr_{0.744}TiO_3$ are cubic (Pm3m) with Ti atom at the center of the cubic Ba/Sr-O structure [41, 42]. Generally, these three phases could be considered as related, where lattice parameter *a* decreases with increase in Sr-content, from around 4.00 Å to around 3.91 Å. Mechanical activation results in a decrease in crystallite size in samples with high Ba and Sr contents,

_____

while it remains relatively constant in the sample with 1:1 Ba:Sr ratio. In the samples with the highest content of $Ba_xSr_{1-x}TiO_3$ phases, microstrain increases with increase in Ba-content.

Additional information on the morphology of precursor powders was obtained using SEM. SEM images show the morphology of precursor powders before and after mechanical activation (Figs 2-4), where mechanically activated powders, in general, exhibit a significant degree of agglomeration. The initial powders (image a in Figs 2-4) show the formation of soft agglomerates, where the finer particles have agglomerated around the larger ones.
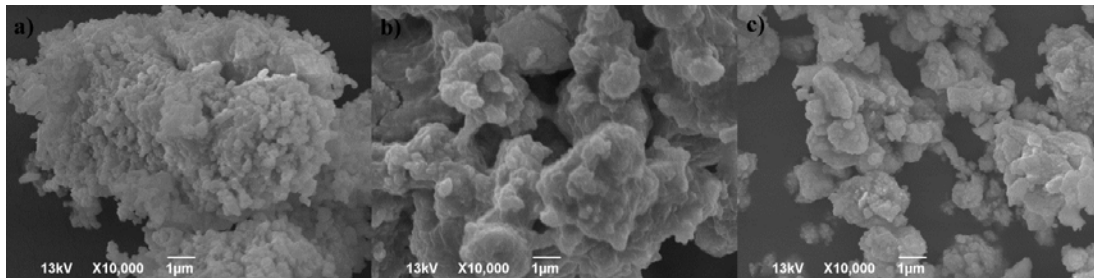
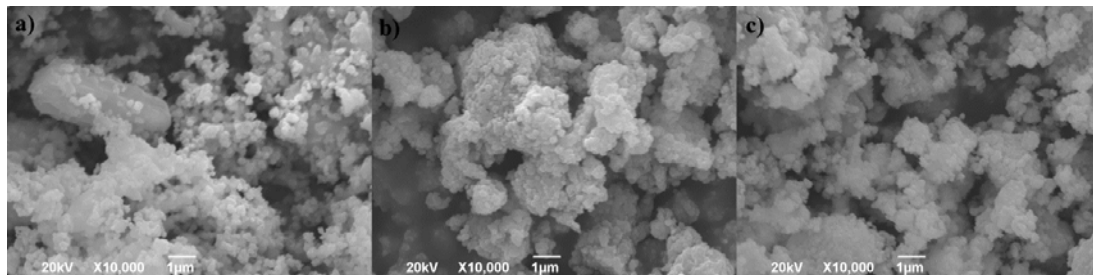**Fig. 2.** SEM images of samples BST82 mechanically activated for (a) 0, (b) 20 and (c) 120 minutes.

Fig. 3. SEM images of samples BST55 mechanically activated for (a) 0, (b) 20 and (c) 120 minutes.
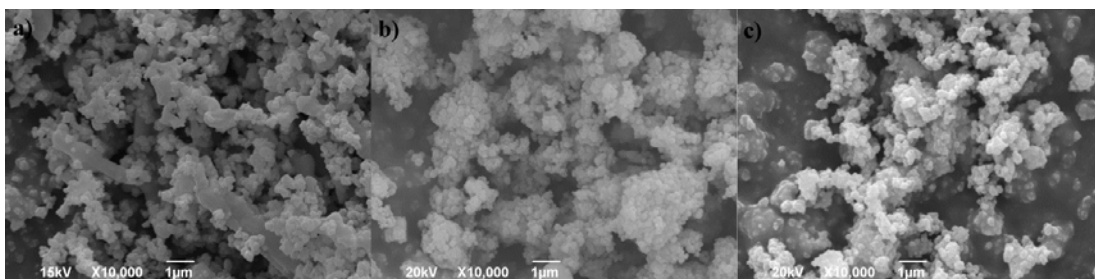

Fig. 4. SEM images of samples BST28 mechanically activated for (a) 0, (b) 20 and (c) 120 minutes.

After 20 min of mechanical activation (image b in Figs 2-4) fragmentation of larger particles and agglomerates takes place. Increase in the number of small particles and formation of the fresh surface due to the breakage of the initial powder particles leads to clustering of smaller particles around larger ones, making the agglomerates themselves smaller and softer. As a result of mechanical activation, there are mass transport processes between the contact surfaces, causing rearrangement of existing and formation of a new phase on the surface of particles. The process is accompanied by agglomeration of smaller particles into larger, as well as the emergence of the new phase, which is harder than the components from which it is

_____

formed. As a result, it can be observed that the powders activated for 120 min (image c in Figs 2-4) appear more homogenous in size, with both smaller particle size and narrower size distribution. This can be correlated with the highest content of the new $Ba_xSr_{1-x}TiO_3$ phase in these samples, where it comprises over 84-92 wt.% of the corresponding samples, where the samples appear to have gone through the process of formation, breaking and reformation of agglomerates during the crystallization of the new phase.

Thermal analysis of powder samples reveals the effect of mechanical activation on the formation of $Ba_xSr_{1-x}TiO_3$ phases. Fig 5 shows DTA curves of non-activated and samples activated for 20 and 120 min. There is a complex endothermic peak in the temperature range of about 800-1000 ^{o}C, corresponding to the formation of a $Ba_xSr_{1-x}TiO_3$ phase. In the sample with 80 % Ba, there is a systematic shift of the maximum of the endothermic peak towards lower temperatures with an increase in mechanical activation – from 935 ^{o}C in the non-activated sample to 925 and 913 ^{o}C in samples activated for 20 and 120 min, respectively. In samples with 50 and 20 % Ba, the difference is more pronounced the peaks of mechanically activated samples both shift to lower temperatures and significantly decrease in intensity, which can be attributed to the increase in the content of $Ba_xSr_{1-x}TiO_3$ phases through mechano-chemical reaction in these samples. In addition, the observed reaction ends much earlier in mechanically activated samples.
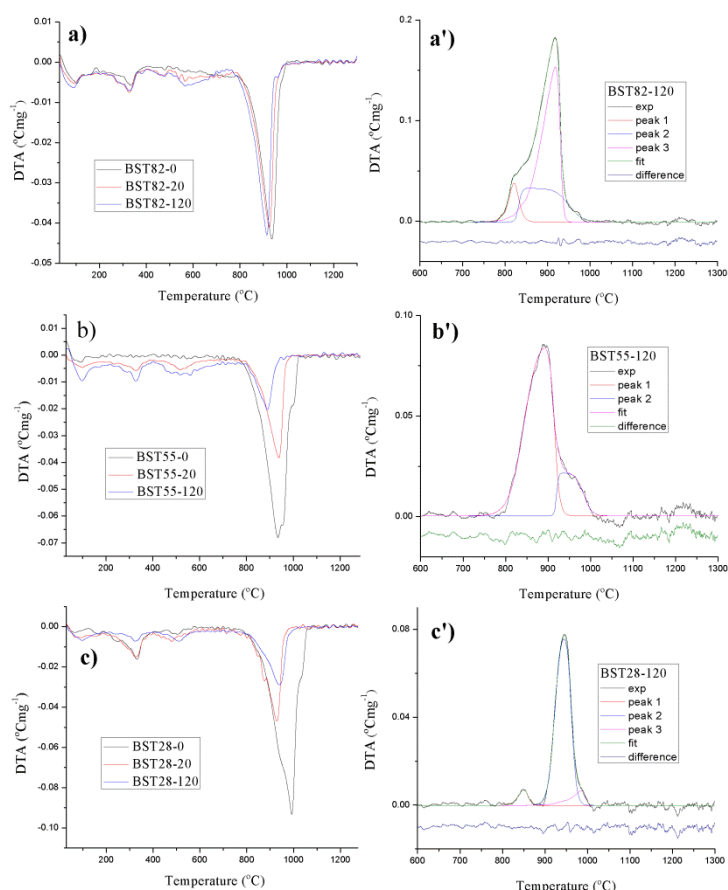

Fig. 5. DTA curves of samples.

Table II shows kinetic data from the deconvoluted endothermic peak in 800-1000 ^{o}C temperature region. Reaction order, Ea and lnk were calculated using the Shishkin method [43]. These results suggest that mechanical activation generally has a significant effect on the activation energy of the formation of $Ba_xSr_{1-x}TiO_3$ phases. It was observed that one peak of

_____

higher activation energy (above 1000 kJmol^{-1}) is present in all samples, which can be correlated with the decomposition of $BaCO_3$ and $SrCO_3$ and consequent diffusion of CO_2 through the sample, resulting in relatively high values of activation energy. As a consequence of smaller particle size after mechanical activation, the activation energy of this peak reduces with increase in time of mechanical activation. The other peaks can be correlated with the formation and crystallization of corresponding $Ba_xSr_{1-x}TiO_3$ phases and the effect of mechanical activation on these processes is generally the reduction in the activation energy. This can be correlated with the state of the sample prior to heating: the formation process of the $Ba_xSr_{1-x}TiO_3$ phase and its crystallization occur easier in samples where particles are smaller and their surface contains more defects as potential nucleation sites for the formation of the new phase. However, the values of some of the processes after 20 and 120 min of activation suggest that agglomeration complicates the kinetics of formation of $Ba_xSr_{1-x}TiO_3$ phases: it should facilitate the reaction within agglomerates, and hinder the reaction between agglomerates, resulting in relatively close values of activation energies for these processes after 20 and 120 min of mechanical activation, respectively.

Tab. II Thermal analysis summary.

Sample	Peak	T (°C)	N	Ea (kJ/mol)	lnk
BST82-0	1	817	0.9	562	53
	2	941	0.7	444	40
	3	966	2.5	2693	295
BST82-20	1	817	0.6	399	37
	2	852	0.6	121	8
	3	929	1.8	1400	152
BST82-120	1	821	0.6	454	43
	2	859	0.9	163	13
	3	919	1.6	1154	125
BST55-0	1	810	3.1	2269	250
	2	945	0.9	292	25
	3	1009	0.8	1472	136
BST55-20	1	824	1.6	1169	126
	2	944	0.5	337	30
BST55-120	1	891	1.0	397	38
	2	936	1.2	457	42
BST28-0	1	812	1.0	3730	372
	2	942	1.1	530	49
	3	1036	0.6	455	40
BST28-20	1	818	1.8	1428	155
	2	933	1.2	782	75
BST28-120	1	850	1.3	1125	118
	2	944	1.3	953	92
	3	985	0.7	669	61

_____

Although the process of mechanical activation has triggered a mechano-chemical reaction of formation of $Ba_xSr_{1-x}TiO_3$ phases, as shown above, the resulting powders have low crystallite size and as such, would be unsuitable for practical application. In order to improve their functional properties, it is necessary to sinter them. Since mechanical activation is known to reduce sintering temperatures and improve the effectiveness of the sintering process [44], the dilatometric study of sintering of mechanically activated powders was performed to determine to what extent this is the case for these $Ba_xSr_{1-x}TiO_3$ systems. The samples were calcined at 800 ^{o}C prior to sintering, in order to remove the remaining carbonates and complete the formation of $Ba_xSr_{1-x}TiO_3$ phases.
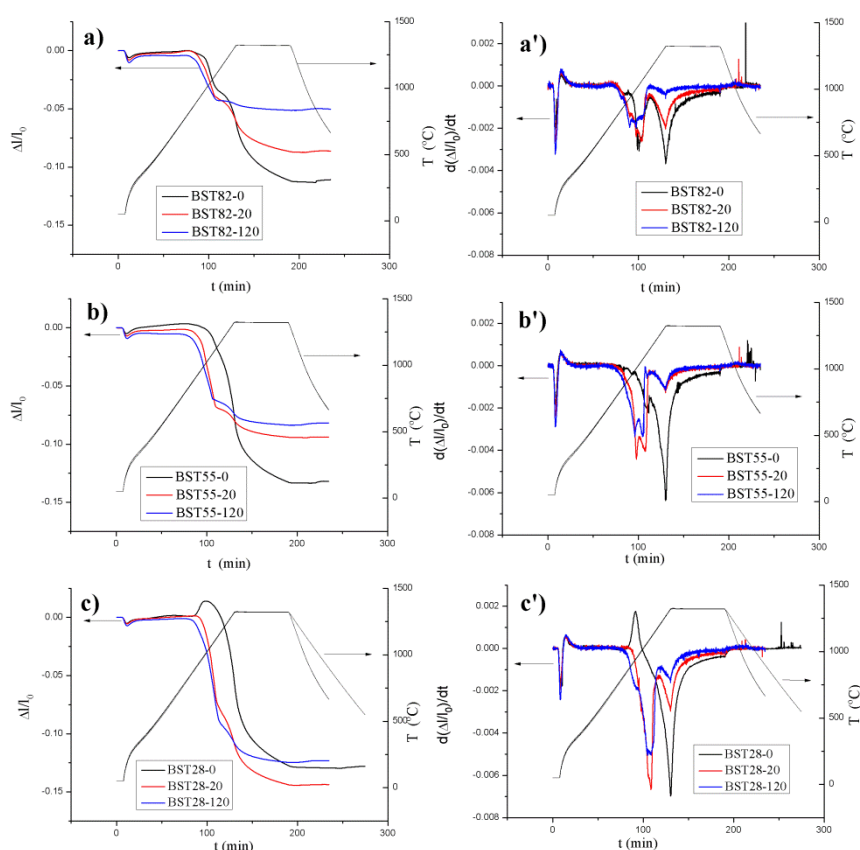

Fig. 6. Dilatometric curves.

Fig. 6 shows dilatometric curves at heating rate 10 ^{o}C for all samples. It can be observed that mechanical activation shifts the onset of the sintering process to lower temperatures for all samples, however, the shift is the smallest for the Ba-rich samples. The process of sintering is generally composed of the part dominated by diffusion and mass transport and the part dominated by recrystallization. The diffusion-dominated part occurs in the non-isothermal portion of the sintering curve, while the transition from non-isothermal to isothermal heating triggers recrystallization. This is evident from the decrease in shrinkage rate on the transition from non-isothermal to isothermal heating.

The initial sintering stage, dominated by mass transport, is complex and can generally be attributed to the formation of the corresponding $Ba_xSr_{1-x}TiO_3$ crystalline phase. There also appears to be an additional superimposed process causing expansion in the sample around 1100 ^{o}C, which is sharper and more pronounced in samples with the lowest Ba content, which can be attributed to the reversible hexagonal-to-cubic phase transformation. The existence of the reversible phase transformation was confirmed by repeated heating of the sintered sample,

where the sample exhibits a visible change in thermal expansion, manifested as a change in the slope of the experimental curve. This phase transformation divides the sample shrinkage into two parts, and Fig. 6 shows how shrinkage rates of mechanically activated samples increase in the first section, while it decreases in the second section. This suggests that higher compactness and homogeneity of the mechanically activated sample powders leads to faster sintering in the first stage, where the highest maximum sintering rate is exhibited by samples activated for 20 min. Lower shrinkage rates in the second section of mechanically activated samples can be attributed to longer diffusion paths in samples that have, at this point, progressed further along. Since the onset of the sintering process for samples activated for 120 min occurs at lower temperatures and the samples are more compact than those activated for 20 min, the same effect can be attributed to the lower shrinkage rates observed in the samples activated for 120 min, compared to those activated for 20 min.
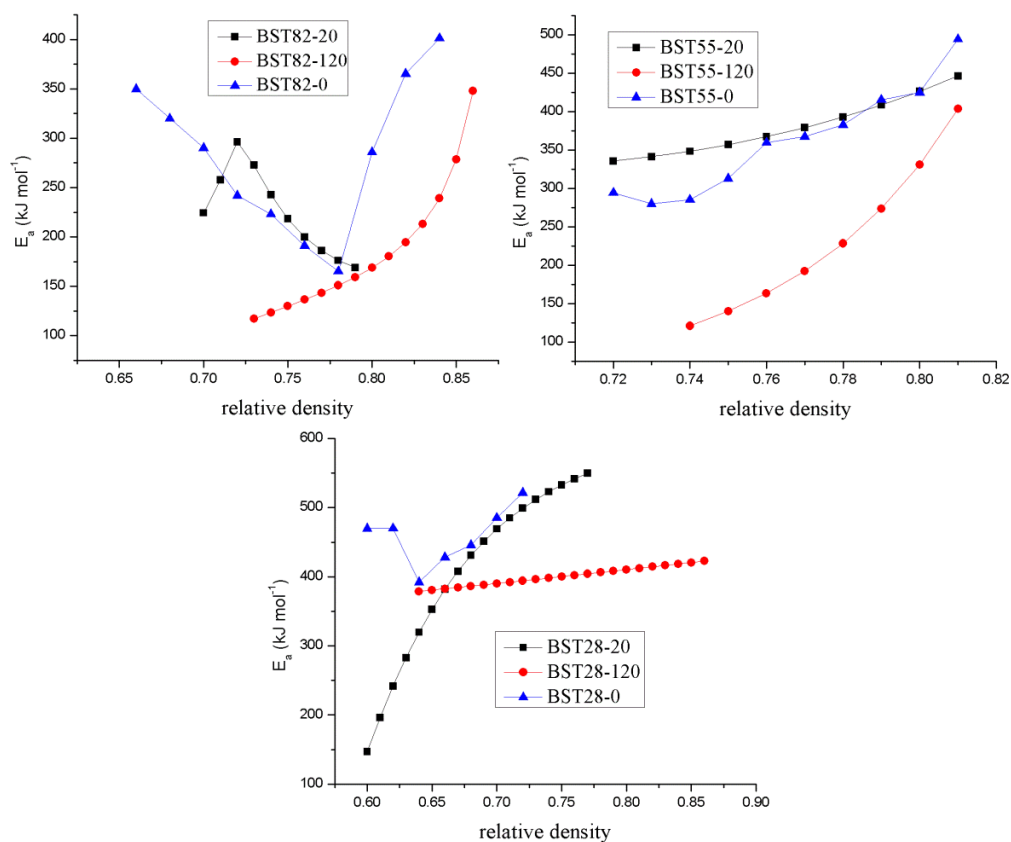

Fig. 7. Values of activation energy (Wang-Raj method).

Fig. 7 shows the values of the activation energy of the sintering process at different values of relative density for mechanically activated samples, determined using Wang-Raj method [45-47]. The changes in activation energy suggest that the mechanical activation facilitates the sintering in the first stage, with the values of activation energies decreasing with increased mechanical activation. Activation for 20 min is much less effective than the one for 120 min due to agglomeration (Fig. 3), which leads to significantly longer diffusion paths between agglomerates. After activation for 120 min, these agglomerates are mostly broken through prolonged mechanical processing, resulting in much more favorable conditions form mass transport during sintering. A general trend of the increase in the values of activation energy at higher values of relative density suggests that there is an increase in the length of diffusion paths as the samples become more compact and particle size increases during

_____

sintering, leading to a higher barrier for further mass transport. Prolonged mechanical activation results in higher relative densities observed both at the beginning and the end of the sintering process, indicating a more compact final product, which is typically associated with improved functional properties [48, 49].
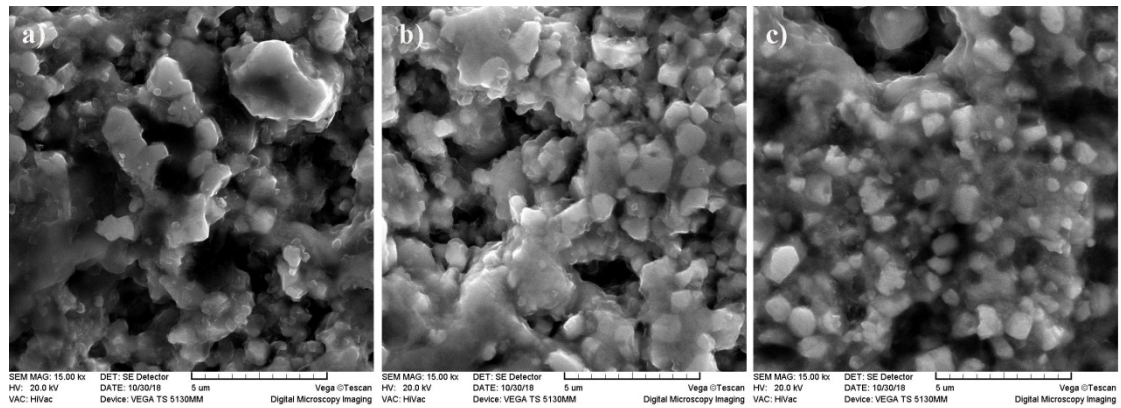

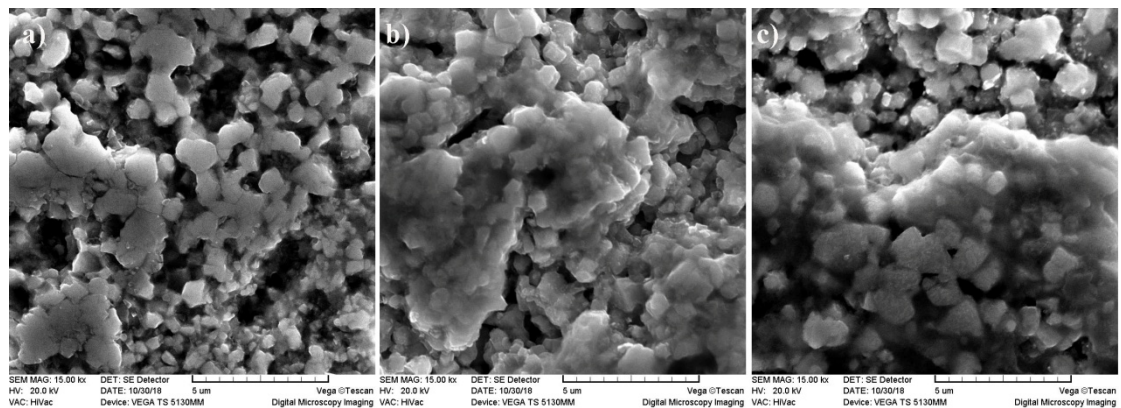**Fig. 8.** SEM images of samples BST82 mechanically activated for (a) 0, (b) 20 and (c) 120 minutes.

Fig. 9. SEM images of samples BST55 mechanically activated for (a) 0, (b) 20 and (c) 120 minutes.
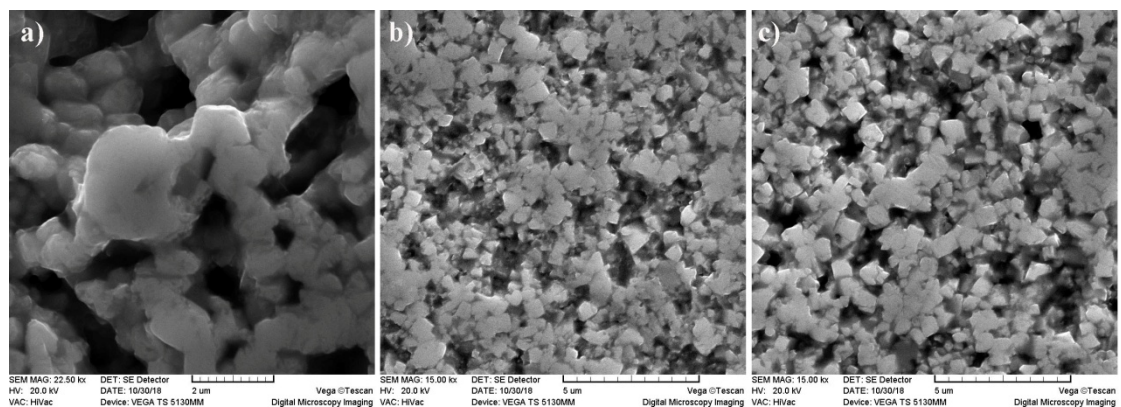

Fig. 10. SEM images of samples BST28 mechanically activated for (a) 0, (b) 20 and (c) 120 minutes.

Morphology of different BST samples with different composition, mechanically activated and sintered, is presented in Figs 8-10. In non-activated sintered samples, early stage of sintering prevails, where necks are formed at the contact points between an adjacent particle and surface diffusion is the dominant mass-transport mechanism (Figs 8-10 a). This is especially pronounced in the samples with 50 and 80 % Sr, which can be attributed to larger particles of $SrTiO_3$ observed in the SEM images of non-activated samples (Fig. 2). Non-activated samples also exhibit significant porosity. After 20 minutes of mechanical activation, the presence of agglomerates, observed in the pre-sintered samples, leads to slower densification process and more inhomogeneous microstructure of sintered samples (Figs 8-10 b). However, compared to non-sintered samples, they are more compact and exhibit lower porosity, although with similar grain size. Mechanical activation for 120 minutes results in most compact samples with the lowest porosity and larger grain size, due to more intense mass transport processes. This can be correlated with smaller grain size and a lower degree of agglomeration observed in pre-sintered samples (Fig. 2). Relatively uniform observed microstructures with a reduced number of pores due to densification should result in better functional properties such as dielectric constant [50].

Generally, samples with the highest barium content exhibit a higher degree of agglomeration and more porous structure, with larger grain size at lower mechanical activation times. At the longest mechanical activation, the sample with 50 % Ba exhibits the highest grain size, which can be attributed to a more compact pre-sintered sample and a lower degree of agglomeration than the sample with 20 % Ba. The sample with highest Sr content consistently exhibits the lowest degree of porosity and the lowest grain size, which is consistent with the state of its pre-sintered powders, which had lower grain size and lower degree of agglomeration compared to the samples with different chemical composition. This indicates that the state of the pre-sintered powder represents the main factor in the morphology of the sintered samples, with mechanical activation providing improved conditions for production of more compact and uniform final product.

4. Conclusion

The influence of mechanical activation on formation, sintering and final morphology of different barium strontium titanate (BST) ceramics was investigated for three different ratios of Ba-to-Sr. It was observed that mechano-chemical reaction occurs in all three BST samples, leading to formation of $Ba_xSr_{1-x}TiO_3$ phases during mechanical activation process. This reaction occurs most readily in the sample with 50% Ba and 50% Sr. Analysis of morphology of mechanically activated powders using XRD and SEM shows that agglomeration is a major limiting factor during mechanical activation, where samples activated for 20 and 120 min show significant degree of agglomeration in SEM and exhibit very little difference in average crystallite size calculated from XRD. This suggests that the activated powders undergo a relatively continuous process of formation and breaking of agglomerates, during which mechano-chemical reaction of formation of $Ba_xSr_{1-x}TiO_3$ phases occurs. Thermal analysis shows that a complex process attributed to formation of $Ba_xSr_{1-x}TiO_3$ phases starts around 800 °C, where mechanical activation generally reduces its activation energy. However, there is relatively little difference in the values of activation energy of mechanically activated samples, indicating that the process of formation of $Ba_xSr_{1-x}TiO_3$ phases is complicated by agglomeration, where mechano-chemical reaction should be facilitated within the agglomerates, but hindered between the agglomerates, due to increase in the length of diffusion paths required for mass transport. Dilatometric study of the sintering of BST samples shows that all samples exhibit a phase transformation around 1100 °C, which can be attributed to the hexagonal-to-cubic phase transition, which persists in sintered ceramics on repeated heating. Sintering kinetics reveals that prolonged mechanical activation

_____

facilitates the sintering process and leads to lower values of activation energies in all BST samples activated for 120 min. Morphology of sintered samples can be correlated mainly to the state of the pre-sintered powder, where more compact powders with lower particle size produced more compact and less porous final sintered product.

Acknowledgments

5. References

1. D. Kosanović, N. Obradović, J. Živojinović, A. Maričić, V. P. Pavlović, V. B. Pavlović, M. M. Ristić, The Influence of Mechanical Activation on Sintering Process of $BaCO_3$-$SrCO_3$-TiO_2 System, Science of Sintering, 44 (3) (2012) 271.
2. O. P. Thakur, Ch. Prakash, D. K. Agrawal, Dielectric behavior of $Ba_{0.95}Sr_{0.05}TiO_3$ ceramics sintered by microwave, Materials Science and Engineering B, 96 (2002) 221.
3. Q. Xu, X.-F. Zhang, Y.-Heng Huang, W. Chen, H.-Xing Liu, M. Chen, B.-Hee Kim, Effect of sintering temperature on structure and nonlinear dielectric properties of $Ba_{0.6}Sr_{0.4}TiO_3$ ceramics prepared by the citrate method, Journal of Physics and Chemistry of Solids, 71 (2010) 1550.
4. H. Abdelkefi, H. Khemakhem, G. Vélu, J. C. Carru, R. Von der Mühll, Dielectric properties and ferroelectric phase transitions in $Ba_xSr_{1-x}TiO_3$ solid solution, Journal of Alloys and Compounds, 399 (2005) 1.
5. Q. Chen, R. Y. Hong, W. G. Feng, Preparation and characterization of composites from $Ba_{0.5}Sr_{0.5}TiO_3$ and polystyrene, Journal of Alloys and Compounds, 609 (2014) 274.
6. A. K. Tagantsev, V. O. Sherman, K. F. Astafiev, J. Venkatesh, N. Setter, Ferroelectric Materials for Microwave Tunable Applications, Journal of Electroceramics, 11 (2003) 5.
7. D. Kosanović, N. Obradović, J. Živojinović, S. Filipović, A. Maričić, V. Pavlović, Y. Tang, M. M. Ristić, Mechanical-Chemical Synthesis $Ba_{0.77}Sr_{0.23}TiO_3$, Science of Sintering, 44 (1) (2012) 47.
8. R. Thomas, V. K. Varadan, S. Komarneni, D. C. Dube, Diffuse phase transitions, electrical conduction, and low-temperature dielectric properties of sol-gel derived ferroelectric barium titanate thin films, J. Appl. Phys., 90 (3) (2001) 1480.
9. Y. C. Liou, C. T. Wu, Synthesis and diffused phase transition of $Ba_{0.7}Sr_{0.3}TiO_3$ ceramics by a reaction-sintering process, Ceram. Int., 34 (2008) 517.
10. S. W. Kim, H. I. Choi, M. H. Lee, J.S. Park, D. J. Kim, D. Do, M. H. Kim, T. K. Song, W. J. Kim, Electrical properties and phase of $BaTiO_3$-$SrTiO_3$ solid solution, Ceram. Int., 39 (2013) 487.
11. X. Q. Liu, T. T. Chen, M. S. Fu, Y. J. Wu, X. M. Chen, Electrocaloric effects in spark plasma sintered $Ba_{0.7}Sr_{0.3}TiO_3$-based ceramics: effects of domain sizes and phase constitution, Ceram. Int., 40 (2014) 11269.
12. S. Inthong, T. Tunkasiri, G. Rujijanagul, K. Pengpat, C. Kruea-In, U. Intatha, S. Eitssayeam, Dielectric, mechanical, and microstructural characterization of HA–BST composites, Ceram. Int., 41 (2015) 481.

13. T. Pečnik, A. Benčan, S. Glinšek, B. Malič, Tailoring the microstructure and dielectric properties of $Ba_{0.5}Sr_{0.5}TiO_3$ thin films by solution-based processing in the frame of the Microstructural Zone Model, Journal of Alloys and Compounds, 743 (2018) 812.

14. Ch. Diao, H. Liu, H. Zheng, Zh. Yao, J. Iqbal, M. Cao, H. Hao, Enhanced energy storage properties of $BaTiO_3$ thin films by $Ba_{0.4}Sr_{0.6}TiO_3$ layers modulation, Journal of Alloys and Compounds, 765 (2018) 362.

15. H. Dong, J. Jian, H. Li, D. Jin, J. Chen, J. Cheng, Improved dielectric tunability of PZT/BST multilayer thin films on Ti substrates, Journal of Alloys and Compounds, 725 (2017) 54.

16. A. Ries, A. Z. Simões, M. Cilense, M. A. Zaghete, J. A. Varela, Barium strontium titanate powder obtained by polymeric precursor method, Materials Characterization, 50 (2003) 217.

17. B. A Wechsler, K. W. Kirby, Phase equilibria in the system barium titanate–strontium titanate, J. Am. Ceram. Soc., 75 (1992) 981.

18. T. Noh, S. Kim, C. Lee, Chemical preparation of barium–strontium-titanate, Bull. Korean Chem. Soc., 16 (1995) 1180.

19. D. Bao, Z. Wang, W. Ren, L. Zhang, X. Yao, Crystallization kinetics of $Ba_{0.8}Sr_{0.2}TiO_3$ sols and sol-gel synthesis of $Ba_{0.8}Sr_{0.2}TiO_3$ thin films, Ceramics International, 25 (1999) 261.

20. J. Wang, X. Yao, L. Zhang, Preparation and dielectric properties of barium strontium titanate glass-ceramics sintered from sol-gel-derived powders, Ceramics International, 30 (2004) 1749.

21. D. Dong, X. Liu, H. Yu, W. Hu, Fabrication of highly dispersed crystallized nanoparticles of barium strontium titanate in the presence of N,N-dimethylacetamide, Ceramics International, 37 (2011) 579.

22. A. Ioachim, M. I. Toacsan, M. G. Banciu, L. Nedelcu, F. Vasiliu, H. V. Alexandru, C. Berbecaru, G. Stoica, Barium strontium titanate-based perovskite materials for microwave applications, Progress in Solid State Chemistry, 35 (2007) 513.

23. H. Yang, Fei Yan, Ying Lin, Tong Wang, Enhanced energy storage properties of $Ba_{0.4}Sr_{0.6}TiO_3$ lead-free ceramics with Bi_2O_3-B_2O_3-SiO_2 glass addition, Journal of the European Ceramic Society, 38 (2018) 1367.

24. [24] X. Wang, Jin-hong Lin, Hong-Yao Zhang, Wei-minGuan, High-porosity $Ba_{1-x}Sr_xTiO_3$ ceramics from particle-stabilized emulsions, Ceramics International, 40 (2014) 10401.

25. J. H. Jeon, Y. D. Hahn, H. D. Kim, Microstructure and dielectric properties of barium-strontium-titanate with a functionally graded structure, J. Eur. Ceram. Soc., 21 (2001) 1653.

26. K. S. Kim, S. H. Shim, S. Kim, S. O. Yoon, Low temperature and microwave dielectric properties of TiO_2/ZBS glass composites, Ceramics International, 36 (5) (2010) 1571.

27. P. Pahuja, C. Prakash, R. P. Tandon, Comparative study of magneto-electric composite system $Ba_{0.95}Sr_{0.05}TiO_3$–$Ni_{0.8}Co_{0.2}Fe_2O_4$ with ferrite prepared by different methods, Ceramics International, 40(4) (2014) 5731.

28. [28] C. L. Mao, X. L. Dong, T. Zeng, H. Chen, F. Cao, Nonhydrolytic sol-gel synthesis and dielectric properties of ultrafine-grained and homogenized $Ba_{0.70}Sr_{0.30}TiO_3$, Ceram. Int. 34 (2008) 45.

29. Q. Xua, X. F. Zhang, Y. H. Huang, W. Chen, H. X. Liu, M. Chen, B. H. Kim, Effect of MgO on structure and nonlinear dielectric properties of $Ba_{0.6}Sr_{0.4}TiO_3$/MgO composite ceramics prepared from superfine powders, J. Alloys Comp. 488 (2009) 448.

30. V. Hornebecq, C. Huber, M. Maglione, M. Antonietti, C. Elissalde, Dielectric Properties of Pure (BaSr)TiO$_3$ and Composites with Different Grain Sizes Ranging from the Nanometer to the Micrometer, Adv. Funct. Mater. 14 (9) (2004) 899.
31. H. F. Zhang, S. W. Or, H. L.W. Chan, Synthesis of fine-crystalline Ba$_{0.6}$Sr$_{0.4}$TiO$_3$–MgO ceramics by novel hybrid processing route, J. Phys. Chem. Solids, 70 (8) (2009) 1218.
32. Q. Chen, R. Y. Hong, W. G. Feng, Preparation and characterization of composites from Ba$_{0.5}$Sr$_{0.5}$TiO$_3$ and polystyrene, Journal of Alloys and Compounds, 609 (2014) 274.
33. U. Gesenhues, Rheology, sedimentation, and filtration of TiO$_2$ suspensions, Chem. Eng. Technol. 26 (2003) 25.
34. H. Miao, Y. Zhou, G. Tan, M. Dong, Microstructure and dielectric properties of ferroelectric barium strontium titanate ceramics prepared by hydrothermal method, J. Electroceram., 21 (2008) 553.
35. A. Z. Simões, F. Moura, T. B. Onofre, M. A. Ramirez, J. A. Varela, E. Longo, Microwave-hydrothermal synthesis of barium strontium titanate nanoparticles, Journal of Alloys and Compounds, 508 (2010) 620.
36. A. Outzourhit, M. A. El Idrissi Raghni, M. L. Hafid, F. Bensamka, A. Outzourhit, Characterization of hydrothermally prepared BaTi$_{1-x}$Zr$_x$O$_3$, J. Alloys Compd., 340 (2002) 214.
37. S. Komarneni, R. Roy, Q. H. Li, Microwave-hydrothermal synthesis of ceramic powders, Mater. Res. Bull., 27 (12) (1992) 1393.
38. S. Komarneni, Q. H. Li, R. Roy, Microwave-hydrothermal processing of layered anion exchangers, J. Mater. Res., 11 (8) (1996) 1866.
39. Y. C. Liou, C. T. Wu, Synthesis and diffused phase transition of Ba$_{0.7}$Sr$_{0.3}$TiO$_3$ ceramics by a reaction-sintering process, Ceramics International, 34 (2008) 517.
40. B. H. Toby, R. B. Von Dreele, GSAS-II: the genesis of a modern open-source all purpose crystallography software package, J. Appl. Crystallogr. 46 (2013) 544.
41. N. B. Mahmood, E. K. Al-Shakarchi, B.Elouadi, Three Techniques Used to Produce BaTiO$_3$ Fine Powder, Journal of Modern Physics, 2 (2011) 1420.
42. Joseph, J., Murthy, V. R. K., Raju, J., Vimala, T. M., Structural investigations on the (Ba, Sr)(Zr, Ti)O$_3$ system, Journal of Physics D, Applied Physics, 32 (1999) 1049.
43. Y. L. Shishkin, Reaction Kinetics Calculated by the Single-Point Method. A Synthesis of the Borchardt-Daniels Theory and the Kissinger Theory of Differential Thermal Analysis, Journal of Thermal Analysis, 30 (1985) 557.
44. L. B. Kong, T. S. Zhang, J. Ma, F. Boey, Progress in synthesis of ferroelectric ceramic materials via high-energy mechano-chemical technique, Progress in Materials Science, 53 (2008) 207.
45. J. Wang, R. Raj, Estimate of the Activation Energies for Boundary Diffusion from Rate-Controlled Sintering of Pure Alumina, and Alumina Doped with Zirconia or Titania, J. Am. Ceram. Soc., 73(5) (1990) 1172.
46. J. Wang, R. Raj, Activation Energy for the Sintering of Two-Phase Alumina/Zirconia Ceramics, J. Am. Ceram. Soc., 74(8) (1991) 1959
47. D. A. Kosanović, V. A. Blagojević, N. J. Labus, N. B. Tadić, V. B. Pavlović, M. M. Ristić, Effect of Chemical Composition on Microstructural Properties and Sintering Kinetics of (Ba,Sr)TiO$_3$ Powders, Science of Sintering, 50 (1) (2018) 29.
48. A. Terzić, N. Obradović, D. Kosanović, J. Stojanović, A. Đorđević, Lj. Andrić, V. B. Pavlović, Effects of mechanical-activation and TiO$_2$ addition on the behavior of two-step sintered steatite ceramics, Ceramics International, 45(3) (2018) 3013.
49. D. Kosanović, V. A. Blagojević, A. Maričić, S. Aleksić, V. P. Pavlović, V. B. Pavlović, B. Vlahović, Influence of mechanical activation on functional properties of barium hexaferrite ceramics, Ceramics International, 44(6) (2018) 6666.

_____

50. Y. Aman, V. Garnier, E. Djurado, Influence of green state processes on the sintering behavior and the subsequent optical properties of spark plasma sintered alumina, J. Eur. Ceram. Soc. 29 (2009) 3363.

Сажетак: *Утицај механичке активације на формирање, морфологију и кинетику синтеровања је испитиван у синтерованој керамици баријум стронцијум титаната (БСТ) са различитим односима баријума и стронцијума. Почетни прахови су механички активирани 20 и 120 минута, што је довело до механохемијске реакције и формирања фаза $Ba_xSr_{1-x}TiO_3$. Утврђено је да агломерација преставља значајан фактор у процесу формирања фаза $Ba_xSr_{1-x}TiO_3$ око 800 ^{o}C и током синтеровања. Она смањује утицај механичке активације на формирање $Ba_xSr_{1-x}TiO_3$ фаза када је активација дужа од 20 минута. Током процеса синтеровања, дужа механичка активација од 120 минута доводи до значајног смањења температуре синтеровања и одговарајуће вредности енергије активације. Такође, сва три система показују фазну трансформацију око 1100 ^{o}C која је приписана прелазу из хексагоналне у кубичну кристалну структуру. Морфологија добијених керамика највише зависи од стања праха пре синтеровања, где механички активирани прахови са мањом величином честица дају компактнији и мање порозни производ.*
Кључне речи: *керамика, синтеровање, кинетика, скенирајућа електронска микроскопија, фазни прелаз.*